

Dwarfism and Increased Adiposity in the *gh1* Mutant Zebrafish *vizzini*

Sarah K. McMenamin,* James E.N. Minchin,* Tiffany N. Gordon, John F. Rawls, and David M. Parichy

Department of Biology (S.K.M., T.N.G., D.M.P.), University of Washington, Seattle Washington 98195; and Departments of Cell Biology and Physiology (J.E.N.M., J.F.R.) and Microbiology and Immunology (J.F.R.), University of North Carolina, Chapel Hill, North Carolina 27599

Somatic growth and adipogenesis are closely associated with the development of obesity in humans. In this study, we identify a zebrafish mutant, *vizzini*, that exhibits both a severe defect in somatic growth and increased accumulation of adipose tissue. Positional cloning of *vizzini* revealed a premature stop codon in *gh1*. Although the effects of GH are largely through *igfs* in mammals, we found no decrease in the expression of *igf* transcripts in *gh1* mutants during larval development. As development progressed, however, we found overall growth to be progressively retarded and the attainment of specific developmental stages to occur at abnormally small body sizes relative to wild type. Moreover, both subcutaneous (sc) and visceral adipose tissues underwent precocious development in *vizzini* mutants, and at maturity, the sizes of different fat deposits were greatly expanded relative to wild type. In vivo confocal imaging of sc adipose tissue (SAT) expansion revealed that *vizzini* mutants exhibit extreme enlargement of adipocyte lipid droplets without a corresponding increase in lipid droplet number. These findings suggest that GH1 signaling restricts SAT hypertrophy in zebrafish. Finally, nutrient deprivation of *vizzini* mutants revealed that SAT mobilization was greatly diminished during caloric restriction, further implicating GH1 signaling in adipose tissue homeostasis. Overall, the zebrafish *gh1* mutant, *vizzini*, exhibits decreased somatic growth, increased adipose tissue accumulation, and disrupted adipose plasticity after nutrient deprivation and represents a novel model to investigate the in vivo dynamics of vertebrate obesity. (*Endocrinology* 154: 1476–1487, 2013)

Energy metabolism and somatic growth are closely coordinated in humans and other vertebrates. For example, childhood obesity is associated with increased linear growth, whereas undernutrition is associated with growth retardation (1). GH is an endocrine factor secreted from the anterior pituitary gland that serves to synchronize growth and metabolism. GH-deficient children exhibit short stature and are mildly obese (2), and supplementation with GH reduces adipose mass in these children (2, 3). In rodents, hypophysectomy (4) or inactivation of a GH transgene (5, 6) leads to obesity independent of food intake. Thus, GH deficiency in mammals is associated with stunted somatic growth and increased adipose tissue (3).

All known effects of GH are mediated through the transmembrane GH receptor (GHR) (7). In mammals, signaling downstream of GHR is mediated by the GHR-associated tyrosine kinase Jak2 (8, 9) and transcriptional activation of *IGF* by Stat5B (10, 11). Indeed, mutations in *GHR*, *JAK2*, *STAT5B*, and *IGF* lead to severe disorders in humans, characterized by GH insensitivity, profound growth failure, short stature, obesity, and increases in specific adipose tissues (review in Ref. 11). GH likely arose early during vertebrate evolution (12, 13), but most of our understanding about GH function derives from studies of humans and other mammals. The activities of GH and IGF in teleost fish appear to be largely conserved with mammals (14, 15). However, the genetic requirements for GH

ISSN Print 0013-7227 ISSN Online 1945-7170
Printed in U.S.A.

Copyright © 2013 by The Endocrine Society
Received July 13, 2012. Accepted January 24, 2013.
First Published Online March 1, 2013

* S.K.M. and J.E.N.M. contributed equally to this work.

Abbreviations: 2D, two dimensional; dpf, days postfertilization; GHR, GH receptor; LD, lipid droplet; qPCR, quantitative RT-PCR; rGH, recombinant chicken GH; SAT, sc adipose tissue; SL, standard length.

on development, growth, and fat storage and mobilization in this group have not been defined. A genome duplication event early in teleost evolution resulted in copies of the *igf* genes, and the zebrafish genome contains *igf1* (also known as *igf1a*), *igf3* (also known as *igf1b*), and *igf2a* and *igf2b* (16). Despite the genome duplication, zebrafish possess only a single gene for GH: *gh1* (17).

In fish as in mammals, white adipose tissue expands via 2 mechanisms: adipocyte hyperplasia (addition of new small fat cells) and adipocyte hypertrophy (growth of existing fat cells) (18). The number and size of adipocytes have important implications for health, because excessive hypertrophy is associated with increased susceptibility to metabolic disorders in humans (19). GH-deficient humans show a reduced number of adipocytes, and this symptom is corrected by GH treatment (20–22). This relationship suggests that GH stimulates adipocyte hyperplasia. However, *in vitro*, the role of GH during adipocyte proliferation is unclear: although GH stimulates adipocyte differentiation of 3T3-F442A cells (23), the hormone inhibits adipocyte differentiation in primary preadipocyte cultures (24, 25). The differential effects of GH on adipose cellularity are linked to the nutritional state of the organism. GH is the major anabolic hormone during nutrient deprivation, increasing lipolysis and stimulating mobilization of stored lipids from adipose tissue (26). Consistent with this role, mammalian tissues deficient for GH show both hypertrophic morphology and reduced rates of lipolysis (20). However, in the fed state, GH exerts acute insulin-like effects by inhibiting noradrenaline-stimulated lipolysis (27). Thus, GH exerts complex and antagonistic effects on adipose tissue growth and morphology relative to nutritional state.

The zebrafish is emerging as an important model for studying developmental endocrinology and adipose tissue metabolism (28–33). As in mammals, zebrafish fat is stored as lipid droplets (LDs) in adipocytes located within multiple, regionally distinct, adipose tissues situated in both visceral and subcutaneous (sc) locations (28, 33). The appearance of these different adipose tissues, or “depots,” is tightly correlated with somatic growth and the attainment of well-characterized postembryonic developmental stages (33, 34). Zebrafish adipocytes share extensive molecular and morphological conservation with mammalian white adipocytes (28, 33), and lipids stored in zebrafish adipocytes are mobilized in response to a negative energy balance (28). Adipocyte LDs can be visualized in live zebrafish using a range of fluorescent lipid dyes (28, 35). Because the defining characteristics of adipocyte hyperplasia and hypertrophy are LD accumulation and growth, longitudinal investigation of LD dynamics provides an account of hyperplastic and hypertrophic adipose growth.

Thus, zebrafish provide a tractable system to investigate GH regulation of both overall somatic development and adipose tissue growth.

In this study, we identify the dwarf zebrafish mutant *vizzini* and map it to a premature stop codon in *gh1*. We show that in the absence of GH1, postembryonic somatic growth, development, and adipogenesis become decoupled, resulting in severely retarded somatic growth, increased adiposity, and an inability to appropriately mobilize stored fats during starvation. Our results provide novel insights into the requirements for GH1 in development, adipocyte morphology, and lipid mobilization in a teleost.

Materials and Methods

Fish rearing, genetic mapping, and genotyping

All experiments using zebrafish were conducted in conformity with the Public Health Service Policy on Humane Care and Use of Laboratory Animals using protocols approved by the Institutional Animal Care and Use Committee of the University of Washington and the University of North Carolina at Chapel Hill. All fish were reared at 28.5°C with a 12-hour light, 12-hour dark cycle. Mutations were induced in the inbred AB^{WP} genetic background by ethyl-N-nitrosourea mutagenesis, and mutant screening was accomplished by early pressure gynogenesis (36). Male *vizzini* produce viable sperm, and females produce small numbers of viable eggs. Mapping families were generated by crossing *vizzini* mutants to the commonly used inbred genetic background *wik*, followed by intercrossing of these F1s to generate a mapping panel of F2 individuals. *vizzini* was assigned to a chromosome by bulked segregant analysis and subsequently mapped at higher resolution using existing and newly developed microsatellite markers. Exons of candidate genes were amplified from genomic DNA, sequenced directly on a 3730 Genetic Analyzer, and compared with sequences derived from the unmutagenized AB^{WP} and other genetic backgrounds. A subset of map cross individuals was subsequently genotyped for a premature stop codon identified within the *gh1* open reading frame by amplifying a 236-bp fragment, then digesting this product to detect an *MseI* restriction site introduced by the presumptive lesion.

Recombinant GH injections

Recombinant chicken GH (rGH) (Sigma, St Louis, Missouri) was reconstituted in sterile ddH₂O at 5 ng/nL. At 38 days post-fertilization (dpf), the smallest fish from a *vizzini*⁺ intercross were selected to enrich for *vizzini* mutants (9/30 fish). These fish were individually housed in glass beakers, and their growth assessed over 9 days. Fish were categorized as mutant or wild-type sibling according to growth during this period; 4 fish were determined to be *vizzini* mutants, and 5 fish were wild-type siblings. In a separate experiment, individual zebrafish of different standard lengths (SLs) were weighed, and quadratic polynomial regression was used to predict body weight from SL (weight in milligrams = $-48.10 + 7.36 \cdot \text{SL} + 0.68 \cdot (\text{SL} - 8.94)^2$, $R^2 = 0.98$). Exogenous injection of 10–100- $\mu\text{g/g}$ body weight rGH induces somatic growth in multiple fish species (37–39). Therefore, 50- $\mu\text{g/g}$ rGH was injected into the abdominal cavity of each

fish every 2 days; SL was recorded after 9 days. Somatic growth over the 9-day period without rGH (–rGH) and with 50- μ g/g exogenous rGH (+rGH) was compared using a paired *t* test.

Analyses of growth and developmental timing

For analyses of growth before the attainment of independent feeding, a homozygous male *vizzini* mutant was crossed with a *vizzini*+ female by in vitro fertilization, and the resulting backcrossed progeny were used for analyses of embryonic growth. Twenty-four individuals were placed in 3% methyl cellulose and imaged at each of 3 stages: 50, 74, and 100 hours after fertilization. Each embryo was genotyped after imaging, and images were measured in ImageJ (40) to determine embryonic length and head-trunk angle (41). Values for head-trunk angle were ln-transformed to correct for heteroscedasticity of residuals; embryonic length and transformed head-trunk angle were analyzed by ANOVA in R (42) to test for effects of age and genotype.

To analyze postembryonic growth, fish from a backcrossed clutch were reared individually in plastic cups and imaged daily. Images were measured in ImageJ for SL and staged according to external anatomical features (34). Differences in the age and SL of wild-type and *vizzini* mutants upon attaining defined stages of postembryonic development were analyzed by ANOVAs to test effects of genotypes, developmental stages, and interaction between the two; tests controlled for repeated measures of individuals (nested within genotypes). Both dpf and SL were ln-transformed to normalize residual variances across factor levels. Independent analyses of the likelihoods of fish attaining specific stages as functions of their genotype, age, SL, and interactions among these variables by multiple logistic regression gave concordant results (details available from D. Parichy on request). Statistical analyses were performed in JMP 8.0 (43).

All imaging was performed with an Olympus SZX-12 stereomicroscope (Olympus, Tokyo, Japan), and digital images were collected with a Zeiss Axiocam HR using Zeiss Axiovision software (Zeiss, Oberkochen, Germany).

Total RNA isolation, cDNA synthesis, primer design, and quantitative RT-PCR (qPCR)

Homozygous and heterozygous *vizzini* siblings were collected at 10 dpf after 4 days of feeding (~10-mm SL). Larvae were anesthetized in MS222, 1–1.5 mm of tail tissue were collected for DNA extraction and genotyping, and the rest of each larva was stored individually in RNAlater (Ambion, Inc, Austin, Texas) while each individual was genotyped. RNA was isolated from 3 *vizzini* homozygotes and 3 heterozygotes and deoxyribonuclease treated using the RNeasy Micro kit (Ambion, Inc) according to the manufacturer's protocol. Superscript III (Invitrogen, Carlsbad, California) was used in cDNA synthesis reactions primed with oligo dT according to the manufacturer's protocol.

Primer sets (forward, reverse, 5' to 3') were designed using Primer3 (44) to span intron-exon boundaries, and each qPCR primer was designed with a 5' tail (AATAAATCATAA) to improve specificity (45). To detect *gh1* transcripts, RT-PCR was performed using primers with the sequence GAAAGCCTC-CGAAAACCAG and GCAGAACGACAGAGGGAAGA. For qPCR, the following primers were used: *igf1a* GTGGAGACAGGGGCTTTTATTT, CTTTGAAAGCAGCATTTCGTC; *igf2a* AGTGTACAGGCTCTTCAACAAG, GATGGGACTC-CTCTCCTTAACC; *igf2b* AAACGTTATGTGGCGGAGAG,

ATCCCACGATTTTGAGAACG; *igf3* GCGGACGAGAAC-TAGTGGAC, CTACGAGCTGCTCCAGGTTT; and *β -actin* AATCCCAAAGCCAACAGAGA, CGACCAGAAGCGTACAGAGA.

RT-PCR to assay the presence of *gh1* transcripts was performed in 25- μ L reactions using 0.25- μ L *Taq* polymerase with 2.5- μ L 10 \times buffer and 0.5- μ L 10mM free deoxyribonucleotides (all from NEB, Ipswich, Massachusetts) with 2- μ L 1:10 diluted cDNA and 0.5 μ L of 10 μ M. Reactions for *β -actin* and *gh1* were amplified simultaneously at 94°C for 3 minutes followed by 30 cycles of 94°C for 30 seconds, 58°C for 30 seconds, and 72°C for 20 seconds, followed by a final step of 72°C for 5 minutes.

qPCR was performed on 3 technical replicates for each of 3 biological replicates. Reactions were performed 25- μ L reaction volumes using 12.5- μ L *Power SYBR Green PCR Master Mix* (Applied Biosystems, Foster City, California), 1.5- μ L specific primer mix (5 μ M) and 3- μ L diluted cDNA. Cycling was performed on a StepOnePlus Real-Time PCR System (Applied Biosystems) with an initial denaturing step at 95°C for 20 minutes followed by 40 cycles of 95°C for 20 seconds, 58°C for 30 seconds, and 72°C for 30 seconds. This was followed by a melt curve stage beginning annealing at 58°C and increasing 3°C with each step. No-template control reactions were performed for each primer set, and all values were normalized to *β -actin*. qPCR data were collected and analyzed using StepOne Software (version 2.1; Applied Biosystems).

Adipose tissue visualization, area morphometrics, and Folch lipid assay

To characterize accumulation of neutral lipids within adipose depots during developmental progression, larvae were reared under standard conditions until they had attained approximately 4.5-mm SL, at which point they were stained with Nile Red as described (28, 35). Images of stained larvae, anesthetized using 0.4 \times MS222 supplemented with 0.003% isoflurane (Baxter, Deerfield, Illinois), were taken using a Leica MZ 16F fluorescence stereomicroscope (Leica, Heerbrugg, Switzerland) equipped with a green fluorescent protein long-pass emission filter set (HQ480/40 \times and HQ510LP), a red-green-blue liquid crystal color filter module, and a Retiga 2000R Fast 1394 cooled digital monochrome camera (QImaging, Tucson, Arizona). Two-dimensional area measurements of pancreatic, abdominal, perirenal (2D), and sc adipose tissues (SATs) were taken in ImageJ and correlated with SL, also measured in ImageJ (32). Adipose areas were assessed by analyses of covariance in JMP testing effects of SL, genotype, an SL \times genotype interaction, as well as repeated measures of individuals (nested within genotypes). Areas were square-root transformed before analysis to correct for differing variances across treatments and sizes.

To determine whether wild-type and *vizzini* mutants reached specific stages of adipose development at significantly different sizes, SLs were analyzed by mixed model ANOVA after ln-transformation to normalize variances in residuals and after controlling for differences attributable to main fixed effects of stage and interactions between stage and genotype, as well as effects attributable to individuals (nested within genotypes).

To generate cross-sections for visualizing gross internal morphology, *vizzini* mutants and size-matched wild-type heterozygotes were fixed with 4% paraformaldehyde and embedded in 4% agarose, then sectioned by vibratome to 400 μ m.

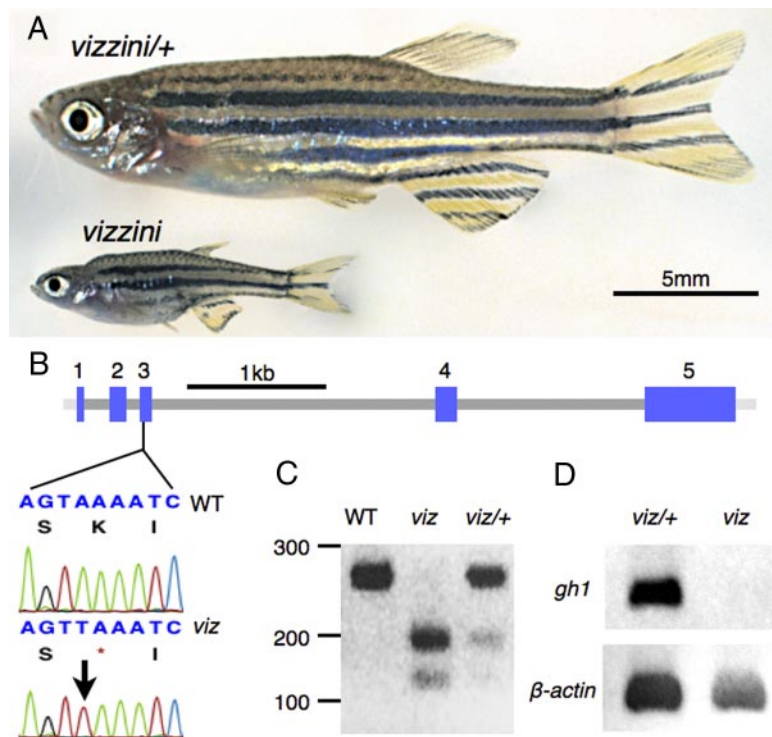


Figure 1. Dwarfism in *vizzini* mutants linked to lesion in *gh1*. (A) Heterozygous and homozygous *vizzini* at their respective full sizes. Scale bar, 5 mm. (B) A→T transversion in the *vizzini* mutant (arrow) introduces a premature stop codon at K64 in the third exon of *gh1*. S, serine; K, lysine; I, isoleucine; * indicates stop codon. (C) Genotyping of individuals using the *MseI* restriction site introduced by the mutation. (D) Transcripts of *gh1* are undetectable in *vizzini* mutants by RT-PCR. WT, wild-type; *viz*, *vizzini* homozygote; *viz/+*, *vizzini* heterozygote.

Total lipid extraction from approximately 10-mm SL wild-type siblings (at ~1 mo of age) and *vizzini* mutants (at ~2.5 mo of age) was performed using the Folch procedure as described (28).

Longitudinal confocal analysis of SAT growth dynamics

To visualize adipose growth at cellular resolution, we used longitudinal in vivo imaging in live animals. Every 6 days, individual wild-type siblings and *vizzini* mutants were stained with the neutral lipid dye, LipidTOX (1:5000; Invitrogen) (35), and their SAT was imaged by confocal microscopy. Superficial SAT was chosen for this analysis, because unlike visceral or perirenal adipose, it can be readily imaged at juvenile stages. At each time point, numbers and sizes of LDs in sc tissues were measured, producing a longitudinal description of LD hyperplasia (Δ SAT-LD#) and hypertrophy (Δ SAT volume) for each animal. Larvae were anesthetized using 0.4× MS222 supplemented with 0.003% isoflurane to facilitate visualization, 1-mg/mL epinephrine (Sigma) was used to condense melanosomes of overlying melanophores. Between imaging time points, larvae were housed within individual wells of a 6-well plastic culture plate; 90% water changes were conducted daily together with scraping, and removal, of debris collecting on the bottom surface of the well. Each fish was fed twice daily with approximately 30 live brine shrimp supplemented with a 3:2 mixture of Golden Pearl powdered food (Brine Shrimp Direct, Ogden, Utah) and spirulina (Aquatic Eco-Systems, Apopka, Florida). LD size and counts

were measured in ImageJ from Z-stacks (635- μ m² field) obtained at the anteriormost extent of the SAT. The 635- μ m² region of interest was kept constant across all time points and fish. LD diameters were ln-transformed before ANOVAs testing effects of genotype, time points and their interaction, and individuals (nested within genotypes).

Nutrient deprivation

Juvenile wild-type siblings and *vizzini* mutants were identified at approximately 2 months of age based on size. Fish were stained with Nile Red, imaged, and then placed in 200 mL of system water in glass beakers. Fish were imaged before starvation (fed state) and days 8 and 21 of starvation. The average size of wild-type siblings was 17-mm SL and *vizzini* mutants 11-mm SL. Body area was measured by tracing the 2D outline of larvae in ImageJ. LD number was quantified within a 1300- × 800- μ m area immediately dorsal to the anus. LD diameters were ln-transformed before ANOVAs as described above.

Results

A premature stop codon within *gh1* causes the *vizzini* phenotype

The recessive, homozygous viable *vizzini* mutant exhibits a severe growth defect. By 6 months after fertilization, wild-type zebrafish have grown to approximately 30-mm SL, whereas homozygous *vizzini* mutants reach only approximately 10-mm SL and never exceed approximately 12-mm SL (Figure 1A). We mapped the *vizzini* mutation to chromosome 3 within 0.9 cM of a microsatellite located in BAC clone AL929222 at 23.5 Mb (18 recombinants of 2112 individuals genotyped). Inspection of this genomic region revealed *gh1* at 22.5 Mb, and sequencing this locus revealed an A→T transversion in the third exon (Figure 1B), resulting in the substitution of a premature stop codon for lysine-64 in the GH1 protein. Sequencing exons from additional candidate genes near AL929222 (*col1a1*, 23.5 Mb; *igf2bp1*, 23.8 Mb; *nr1d1*, 23.8 Mb; and *zgc:73293*, 23.9 Mb) failed to reveal either missense or nonsense mutations. To further test cosegregation of the *vizzini* mutant phenotype and *gh1* lesion, we genotyped 370 individuals (including 18 individuals recombinant between *vizzini* and the microsatellite within AL929222) for the presence of the *gh1* A→T transversion, using an *MseI* restriction site introduced by the lesion. These analyses revealed no recombinants, consistent with allelism of *vizzini* and *gh1* (see Figure 1C). The premature stop codon within *gh1* was

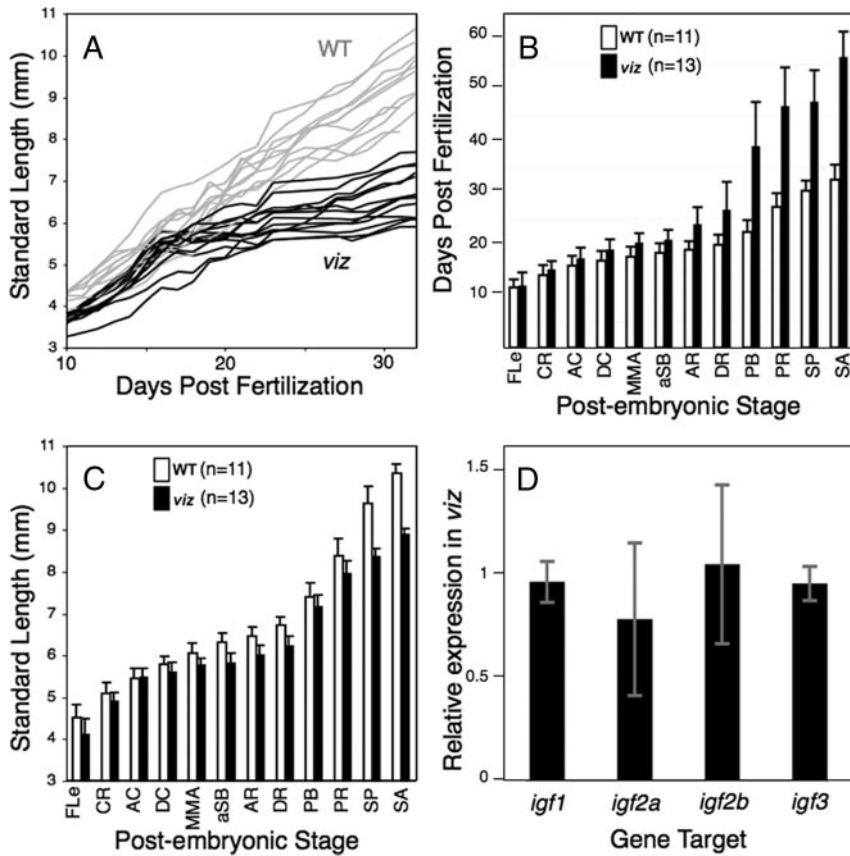


Figure 2. *vizzini* mutants show decoupled growth and development but similar *igf* expression at an early stage. (A) In comparison with their wild-type *vizzini*^{+/+} siblings (gray), *vizzini* mutants (black) exhibited retarded growth beginning shortly after first feeding. (B and C) Relationships between developmental stage and age (B) and developmental stage and size (C) differed between *vizzini* mutants and wild-type siblings. X-axes show developmental milestones describing early larval stages (left) through late larval stages (right) as defined in Ref. 34. (B) *vizzini* mutants (black bars) took longer to reach defined developmental stages than their wild-type siblings (open bars; $F_{1,24} = 43.1, P < .0001$), and the magnitude of this difference was increasingly severe at later stages (stage x genotype interaction, $F_{12,598} = 32.1, P < .0001$). (C) *vizzini* mutants also were smaller than their wild-type siblings upon reaching defined developmental stages ($F_{1,28} = 48.0, P < .0001$), with differences greater at later stages (stage x genotype interaction, $F_{12,606} = 5.2, P < .0001$). $N = 642$ observations, 24 individuals. Stages as described in Ref. 34; FLe, notochord flexion; CR, caudal fin ray appearance; AC, anal fin condensation; DC, dorsal fin condensation; MMA, metamorphic melanophore appearance; aSB, inflation of anterior swim bladder lobe; AR, anal fin ray appearance; DR, dorsal fin ray appearance; PB, pelvic fin bud appearance; PR, pelvic fin ray appearance; SP, squamation through posterior; SA, squamation through anterior. Bars indicate means \pm 1 SEM. WT, wild-type; *viz*, *vizzini* mutants.

predicted to result in nonsense-mediated mRNA decay and reduced levels of *gh1* transcript in *vizzini* mutants as compared with the wild type; this prediction was confirmed by RT-PCR (Figure 1D). Additionally, we tested whether injection of exogenous rGH could rescue growth in *vizzini* mutants. Repeated injection with rGH induced a significant increase in growth of mutants ($P < .01$) (Supplemental Figure 1, published on The Endocrine Society’s Journals Online web site at <http://endo.endojournals.org>), demonstrating that exogenous rGH is sufficient to rescue

somatic growth in *vizzini* mutants. Together, these data support the conclusion that the *vizzini* phenotype results from a premature stop codon in the zebrafish orthologue of the GH gene, *gh1*.

Somatic growth decoupled from development and age in *vizzini* mutants

To assess roles for *gh1* in zebrafish development, we compared growth and developmental progression of wild-type and *vizzini* mutant individuals from embryonic through larval and adult stages. Before the onset of independent feeding, *vizzini* mutant embryos and early larvae (50, 74, and 100 hours postfertilization) developed at a rate statistically indistinguishable from the wild type, reminiscent of the GH1-independent growth during embryonic, fetal, and early postnatal periods in humans (46). Nevertheless, size differences became apparent after the onset of feeding (5 dpf) and were increasingly pronounced with age (Figure 2A). To determine whether *gh1* promotes developmental progression in addition to growth, we assessed the appearance of morphological features diagnostic for different postembryonic stages (34). We predicted that if developmental events are promoted by GH1 signals, or if different developmental events exhibit differential GH1 dependencies, then *vizzini* mutants might exhibit heterochronic changes in stage progression, with disordered or delayed appearance of developmental

milestones. We found that stage-specific milestones appeared in their normal order in *vizzini* mutants but that stages were attained at progressively older ages than in wild-type fish (Figure 2B). Nonetheless, stages of development were reached by mutants at sizes somewhat smaller than those of wild-type controls (Figure 2C and Supplemental Figure 2). Thus, in the absence of *gh1*, fish growth was retarded relative to age, but developmental stage was advanced relative to size.

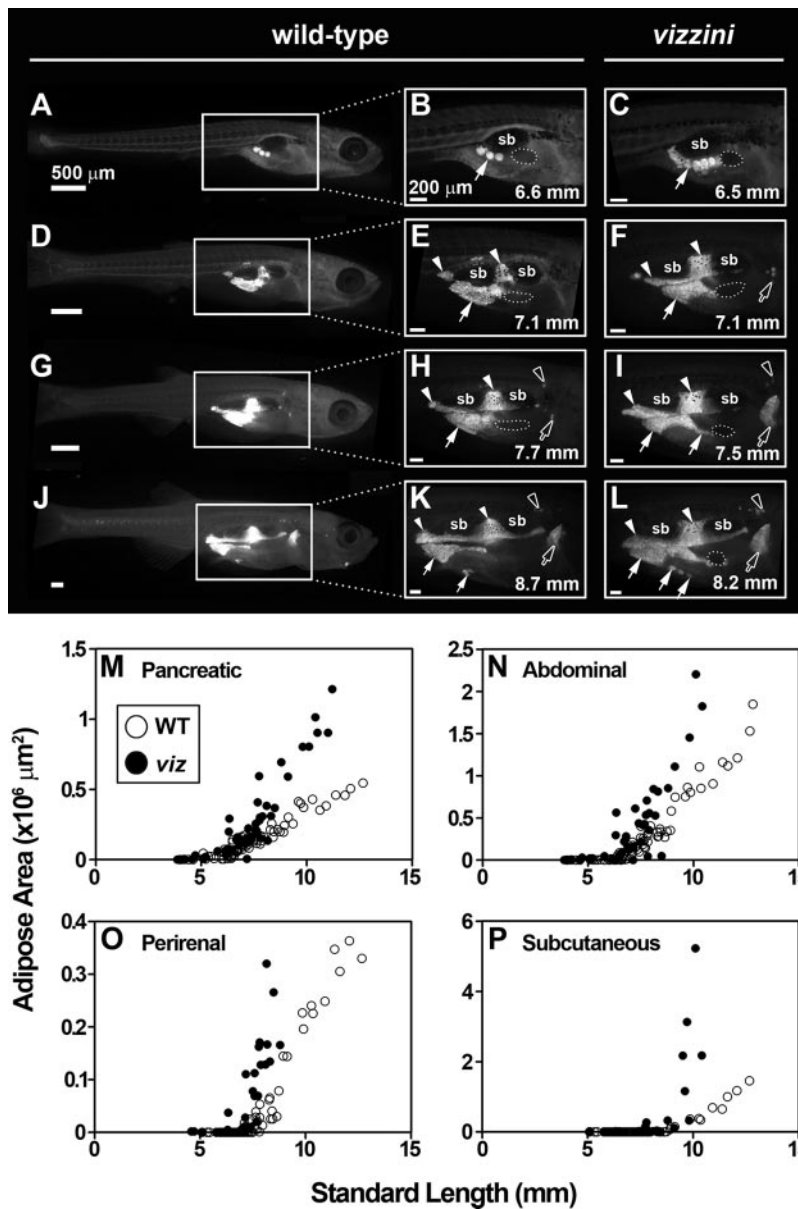


Figure 3. *vizzini* mutants exhibit greater size-specific adiposity than wild-type larvae. (A–L) Images of Nile Red-stained neutral lipid in wild-type and *vizzini* mutant larvae. Wild-type siblings (A, B, D, E, G, H, J, and K) undergo expansion of pancreatic (arrows), abdominal (arrowheads), and perirenal (open arrows) adipose tissues. These depots are larger in equivalently sized *vizzini* mutants (C, F, I, and L). sb, swim bladder; white dotted outline, gall bladder. (M–P) Quantification of adipose depot areas reveals that at a given SL, *vizzini* mutants exhibit significantly greater adiposity than the wild type, as evidenced by significant SL \times genotype interactions (M, $F_{1,93} = 171.2$; N, $F_{1,106} = 173.1$; O, $F_{1,93} = 161.4$; P, $F_{1,33} = 23.8$; all, $P < .0001$; $N = 446$ observations; 20 wild-type, 20 *vizzini* mutants). WT, wild-type; viz, *vizzini* mutants.

No detectable change in *igf* expression in *vizzini* mutants at 10 dpf

In mammals and in fish, the growth-promoting effects of GH are mediated by GH-dependent transcriptional regulation of IGF family genes (47–50). To investigate GH1 regulation of IGF expression in zebrafish, we used qPCR to compare expression of *igf* genes between wild-type and *vizzini* mutants at 10 dpf (~4-mm SL), when overall mor-

phological defects in mutants were still relatively subtle (see Figure 2A). These analyses did not reveal significant differences in *igf* gene expression between *vizzini* mutants and their heterozygous siblings at this early stage, although overall expression levels were low (delta threshold cycle = 4.8–11.1), limiting our power to detect subtle differences that might have been present (Figure 2D).

vizzini mutants exhibit obesity

GH regulates adiposity in mammals (51, 52), and our identification of *vizzini* as a *gh1* mutant provided the opportunity to test whether GH1 regulates adipose development or accumulation in zebrafish. To test these possibilities, we visualized neutral lipids in live *vizzini* mutants and siblings (28, 35). The first zebrafish adipocyte LDs appear in a visceral location associated with the pancreas (Figure 3, A and B) (28, 33). LDs next develop intra-abdominally, associated with the swim bladder (Figure 3, D and E), followed by perirenal (Figure 3, G and H) and sc locations (Figure 3, G and H). Consistent with analyses of postembryonic stages (Figure 2C), *vizzini* mutants attained specific stages of adipose development in their normal order but attained these stages while smaller and older than wild-type siblings (Supplemental Figure 3). We conclude that GH1 is not required for establishing adipose tissue depots nor for initiating morphogenetic events that characterize these depots.

To test whether GH1 regulates the accumulation of lipids within adipose depots, we measured 2D areas

of depots during larval growth. Comparing *vizzini* mutants and size-matched wild-type larvae revealed substantially more adipose tissue in the mutants (Figure 3, A–L). Moreover, the 2D areas of the four examined adipose tissues became increasingly large relative to size-matched wild-type individuals as body length increased (Figure 3, M–P). In larger larvae (eg, 10.1-mm SL), both ventral ab-

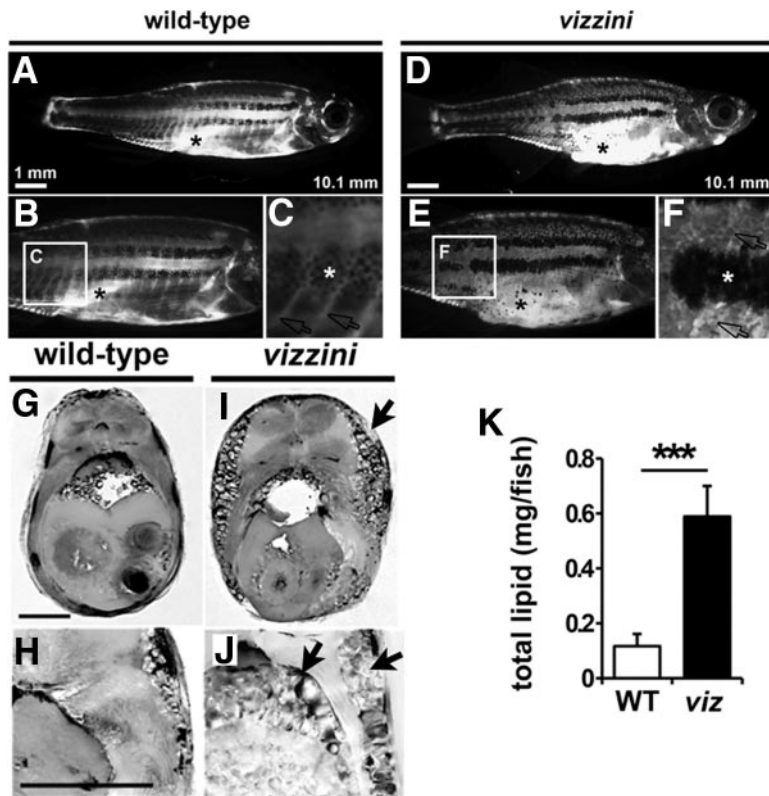


Figure 4. Increased visceral and SAT in late larval *vizzini* mutants. Images of Nile Red-stained neutral lipid in wild-type siblings and *vizzini* mutant zebrafish (A–F). Cross-sections through trunk of wild-type and *vizzini* mutants (G–J). (A–F) Nile Red fluorescence (white signal) is increased in both visceral (asterisks, A and D) and SAT (arrows, C and F) in *vizzini* mutants. White asterisks denote melanophores of the adult pigment stripes. (G–J) Visceral and SAT, visible as globular LDs, is increased in *vizzini* mutants (arrows in I and J). Region shown is just anterior to that shown in C and F. Scale bar, 1 mm. (K) Folch extraction significantly increased total lipid in *vizzini* mutants (wild-type sibling, $n = 4$; *vizzini* mutants, $n = 5$). Student's t test, $P < .0001$. Bars indicate means \pm 1 SEM. WT, wild-type; viz, *vizzini* mutants.

dominal and SATs were markedly expanded in *vizzini* mutants compared with the wild type; indeed, we found lipids to be ectopically deposited along the entire flanks of mutants (Figure 4, A–F). The expansion of adipose tissue was clearly apparent even in unstained transverse sections (Figure 4, G–J). Measurement of absolute lipid levels after Folch extraction further demonstrated significantly increased lipid contents of *vizzini* mutants compared with size-matched wild-type controls (Figure 4K). These findings demonstrate that for a given size, *vizzini* mutants exhibit increased amounts of adipose tissue compared with wild type, and confirm roles for GH1 in the regulation of both sc and visceral adiposity in zebrafish.

Increased LD hypertrophy in *vizzini* mutants

GH is implicated in regulating mammalian adipose morphology through both hyperplastic and hypertrophic mechanisms (53, 54). To determine whether zebrafish GH1 plays a role in adipocyte hyperplasia and hypertrophy in vivo, we used fluorescent lipid dyes to label adi-

pocyte LDs (28, 35) and performed longitudinal confocal live imaging to visualize changes in LD number and size in SATs in wild-type and *vizzini* mutant larvae (Figure 5, A–E). Mature adipocytes contain a single large LD, and the number and size of LDs serve as a proxy for hyperplasia and hypertrophy, respectively (35, 55). These cellular-level confocal analyses of longitudinal in vivo adipose morphology and dynamics in zebrafish provide a complement to existing mammalian in vivo imaging techniques, including nuclear magnetic resonance, bioluminescence, and computed tomography (54, 56, 57).

Over the course of the observational period, individuals exhibited expected levels of somatic growth, indicative of overall good health (Supplemental Figure 4). In wild-type siblings, SAT LDs increased both in size and number (Figure 5, F and G), demonstrating that SAT growth is derived both from adipocyte hypertrophy and hyperplasia. Strikingly, *vizzini* mutants exhibited a significantly increased diameter of sc LDs compared with the wild type (Figure 5F), suggesting that GH1 normally constrains hypertrophy. By contrast, *vizzini* mutants did not exhibit a significant change in LD number in comparison with the wild type (Figure 5G). Taken together, in vivo imaging reveals that GH1 deficiency in zebrafish causes hypertrophic expansion of SAT

without increasing LD number. These results are consistent with the enlargement of sc adipocytes observed in GH-deficient humans (20) and the increased sc adipose mass in dwarf mouse lines with disrupted GH signaling (58), suggesting that GH1 plays an analogous role in regulating adipocyte morphology in fish as in mammals.

Adipose stores in *vizzini* mutants resistant to mobilization during starvation

During starvation in mammals, GH stimulates lipolysis and mobilization of lipids stored within adipose tissues (26). Because of the enlarged sc adipocyte LDs observed in *vizzini*, we hypothesized that GH1 functions in lipid mobilization in zebrafish. To test lipid mobilization in response to a negative energy balance, juvenile wild-type and *vizzini* mutants were starved for 21 days (Figure 6). In wild-type siblings, the number of LDs within SATs decreased during nutrient deprivation and were often undetectable after 21 days of starvation (Figure 6, A–F). Con-

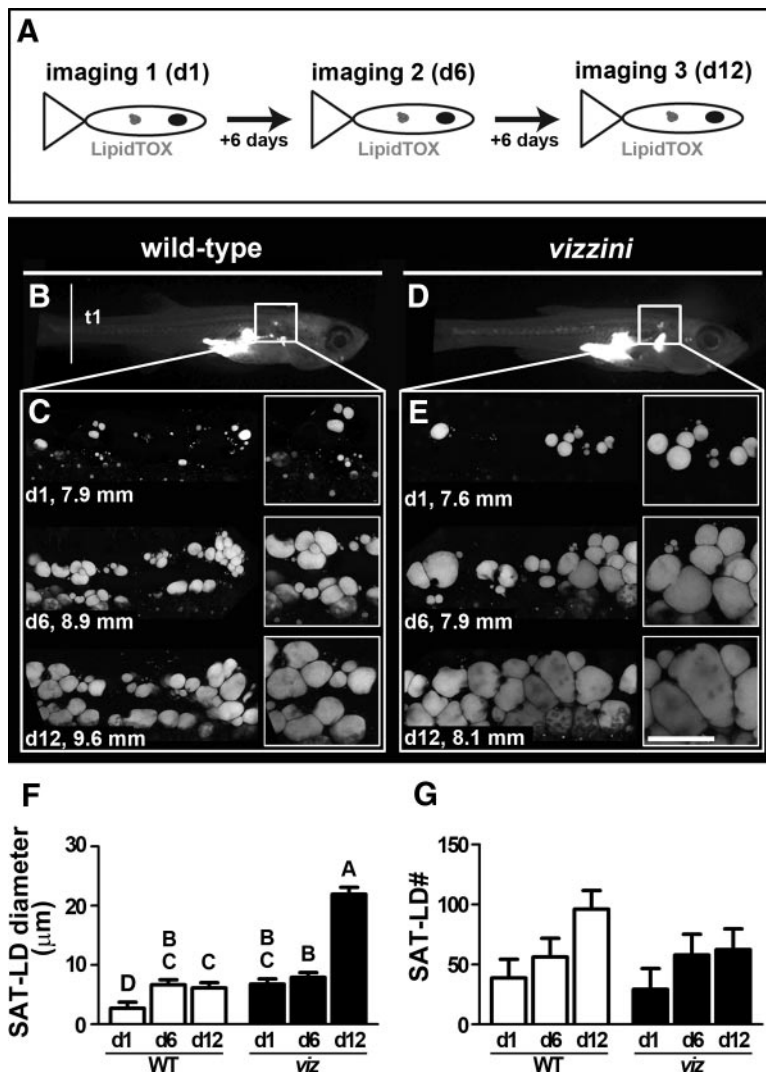


Figure 5. Longitudinal confocal imaging of SAT growth in wild-type and *vizzini* mutant siblings. Confocal imaging of LipidTOX-stained SAT in wild-type sibling (B and C) and *vizzini* mutants (D and E). (A) Schematic of imaging procedure. Animals were imaged 3 times at 6-day intervals (d1, day 1; d6, day 6; d12, day 12). (B–E) Wild-type sibling (B and C) showing progressive SAT growth over 3 time points. *vizzini* mutant showing extreme SAT-LD hypertrophy over 3 time points (D and E). Regions within white boxes are shown at higher magnification. (F) Average LD diameter varied among time points ($P < .0001$), and *vizzini* mutants exhibited larger LD diameters than wild-type, particularly evident at the final time point (as evidenced by a significant genotype \times time-point interaction, $F_{2,1538} = 37.4$, $P < .0001$). Groups with the same letters are not significantly different ($P > .05$) by Tukey honestly significant difference test. (G) Mean number of LDs exhibited an overall increase at later time points ($F_{2,24} = 4.9$, $P < .05$) but did not differ significantly between genotypes ($F_{1,25} = 0.9$, $P = .4$), nor did differences between time points depend on genotype (genotype \times time point interaction, $F_{2,21} = 0.6$, $P = .6$); accordingly, post hoc pairwise comparisons of genotype, and time point means revealed no significant differences, although when genotypes were combined, d12 means were significantly greater than d1 means. Scale for all white outlined boxes is 100 μm . Bars indicate means \pm 1 SEM. $N = 5$ wild-type, 4 *vizzini* mutants. WT, wild-type; viz, *vizzini* mutants.

cordantly, the size of the remaining LDs decreased over the course of nutrient deprivation (Figure 6, M and N). In contrast, sc lipids in *vizzini* were not mobilized even after 21 days of starvation (Figure 6, G–L), we observed no measurable reduction in either the size or number of LDs

(Figure 6, M and N). Thus, we conclude that GH1 deficiency impairs the mobilization of sc lipid stores during zebrafish nutrient deprivation.

Discussion

In this study, we demonstrate that dwarf *vizzini* mutant zebrafish harbor a premature stop codon in *gh1*, identifying the first loss-of-function GH fish, and we determined that GH1 serves as an essential regulator of size and adiposity in zebrafish. Overexpression of GH1 can substantially increase growth rate and is thus a frequent target for agricultural biotechnology. Indeed, the molecular targets and physiological effects of GH are important in an aquaculture context, and transgenic lines with exogenous GH genes have been established in a number of commercially important fish species, including tilapia and salmon (59–61). Moreover, GH is an important regulator of lipid metabolism in humans, and understanding the cellular roles of this hormone is applicable to the worldwide obesity epidemic. Other teleosts and mammals (including humans) have a second, extrapituitary GH gene (3, 62, 63). In contrast, zebrafish possess only a single GH gene, *gh1* (17), allowing us to scrutinize development and lipogenesis in the absence of any potential compensatory effects of a GH homologue (note however that other members of the GH/prolactin family may bind to GHRs) (17). Moreover, the zebrafish model offers unrivaled potential for visualizing vertebrate tissue dynamics, and we have used this capability to evaluate lipid fluctuations at a cellular level in both wild-type fish and in the absence of GH.

Although the pituitary gland begins expressing *gh1* at 2 dpf (64), we found no effect of *gh1* loss-of-function on embryonic and early larval growth before feeding. This result corroborates previous findings of GH-independent growth during embryonic and early larval development of zebrafish (65) and during the early postnatal period of humans (46). However, the consequences of GH1 deficiency became apparent during later larval development, and significant size differences

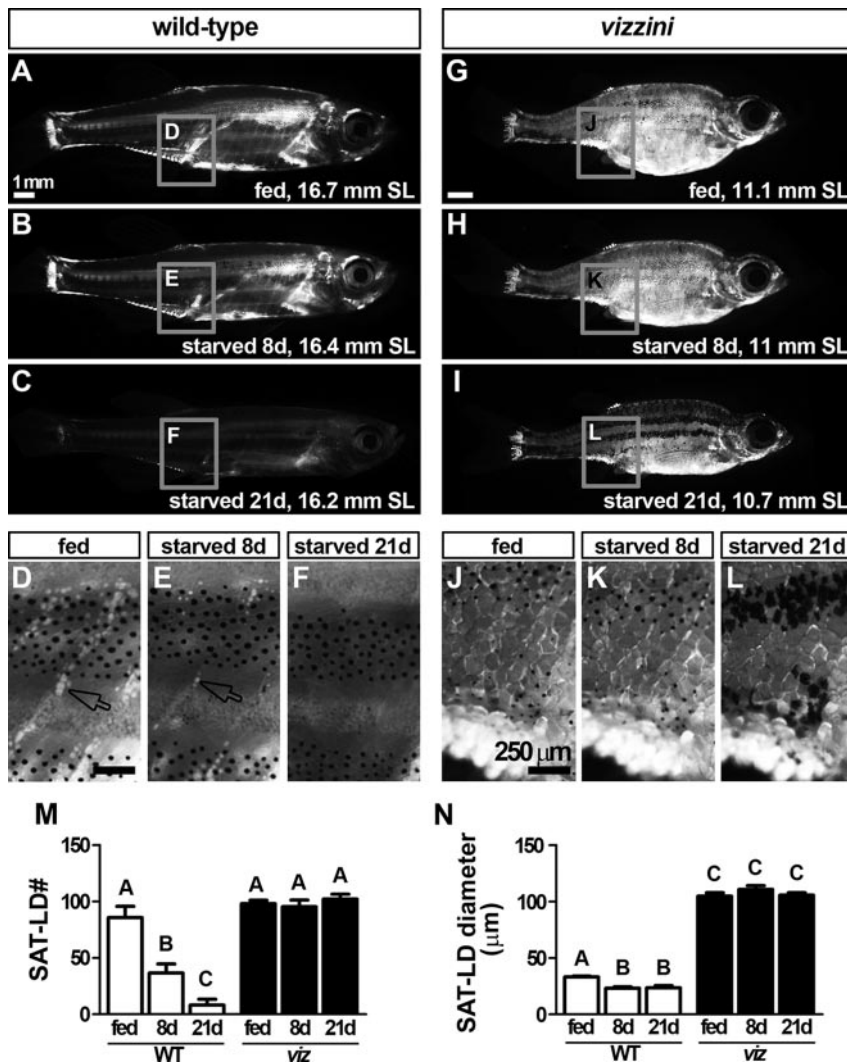


Figure 6. *vizzini* mutants exhibit reduced SAT mobilization during nutrient deprivation. Images of Nile Red-stained wild-type and sibling *vizzini* mutants (A–L). (A–F) Images from a representative wild-type sibling during the course of 21 days of starvation. Note overall reduction in Nile Red stain between A and C. SAT-LDs gradually disappear during nutrient deprivation (arrows, D–F). (G–L) Images from a representative *vizzini* mutant, illustrating increased SAT during the fed state (G and J) and failure of SAT-LD reduction during starvation (I and L). (M) Mean SAT-LD diameter decreased slightly in wild-type larvae upon starvation but did not change significantly with starvation in *vizzini* mutants (genotype x time point interaction, $F_{2,1945} = 175.2, P < .0001$). (N) Lipid SAT-LD number decreased after 21 days of starvation in wild-type siblings but not in *vizzini* mutants (genotype x time point interaction, $F_{2,27} = 4.5, P < .05$). In M and N, bars are means \pm 1 SEM, with letters indicating means not significantly different ($P > .05$) by Tukey honestly significant difference comparisons. $N = 6$ wild-type, 5 *vizzini* mutants. WT, wild-type; viz, *vizzini* mutants.

were manifested between homozygous *vizzini* mutants and wild-type siblings by 10 dpf, becoming increasingly severe as development progressed. It is well established that the GH-IGF axis regulates postembryonic somatic growth in mammals (66, 67). However, we found that whole-fish expression levels of *igf* transcripts were comparable between *vizzini* mutants and heterozygous siblings at 10 dpf, suggesting that IGF expression may be GH independent at these stages in zebrafish. Nonetheless, expression levels at this early stage were low for each of the

genes in both wild types and mutants, and this may have precluded the detection of any subtle *gh1* dependencies. Analyses of tissue-specific *igf* gene expression profiles at later stages would be informative for further testing roles for the GH-IGF axis in regulating zebrafish growth.

Developmental progress is highly correlated with size in zebrafish, and size alone predicts the state of most developmental traits with over 90% accuracy (age is far less predictive of developmental stage) (34). To test whether GH1 is required to maintain this close relationship between size and stage, we compared developmental states in mutants with those in age-matched wild-type fish. We found that the order in which anatomical somatic milestones appear is unaffected by the lack of *gh1* in zebrafish, suggesting that GH1-independent mechanisms regulate postembryonic developmental progress. Even so, because *vizzini* mutants grow much more slowly than normal fish, developmental stages are attained at older ages than in wild type. Our results therefore indicate that GH1 is not essential for developmental progression and that GH1-independent mechanisms promote the appearance of stage-specific markers after a requisite developmental state or minimum overall size is reached.

We submit the *vizzini* mutant as a useful new model for understanding vertebrate obesity. Our data demonstrate that adipose tissue is increased and adipose development is ad-

vanced relative to size in *vizzini* mutants. Thus, *vizzini* mutants satisfy the common criterion of being overweight or obese: increased adipose tissue relative to a linear measure of size (height in humans, SL in zebrafish). In contrast to mammalian obesity models, the zebrafish system offers excellent potential for high-resolution in vivo imaging, and our study addresses long-established technical limitations concerning in vivo imaging of adipose tissue. Several approaches have been developed to study adipose tissue dynamics in mammals, including ex vivo culture of

adipose tissue, intravital confocal microscopy after surgical incision and coverslip implantation, and mathematical modeling using data from reiterated adipose biopsies (68–72). These approaches have provided novel paradigms in adipose growth, particularly in the context of differing endocrinological contexts; however, these methods are inherently invasive and do not permit visualization of cellular dynamics within the intact physiological context of in vivo adipose tissue. To our knowledge, this study provides the first noninvasive and longitudinal visualization of in vivo adipose tissue formation and growth.

In this study, we demonstrated that *vizzini* mutants have increased sc and visceral adipose tissue relative to body size. The observed increase in sc adiposity is similar to that exhibited by GH-deficient mouse models, including an ethyl-N-nitrosourea-induced missense *Gh^{sma1}* mutation (73), a *Ghr* mutant (58, 74), and the Snell dwarf line, in which development of the anterior pituitary gland is disrupted (75, 76). Similarly, GH-deficient and GH-insensitive humans develop abnormally large amounts of SAT (77–79). Thus, it appears that GH has a conserved role in regulating lipid storage within SAT from humans to zebrafish. GH-deficient mouse models exhibit visceral depot-specific responses to GH. Retroperitoneal adipose was increased in GHR mutants (58); however, epididymal adipose was either unchanged (58, 80) or reduced (81) when normalized to body weight. *Gh^{sma1}* mutants exhibit increased visceral adipose tissue; however, it is unclear which visceral adipose tissue was analyzed (73). In *vizzini*, 3 independent visceral adipose tissues (pancreatic, abdominal associated with the swim bladder, and perirenal) were larger relative to body length. Therefore, our data are consistent with a role for GH in regulating the size of visceral adipose tissue.

We found that the increased overall size of the SAT was caused by a dramatic increase in the size of adipocyte LDs. GH impairment in mammals is characterized by large sc adipocytes (2–4), suggesting a role for GH in regulating the size of adipocytes in both mammals and teleosts. The role of GH in regulating the number of adipocytes within adipose tissue is less clear. Although GH-deficient humans show reduced numbers of sc adipocytes and increase the number of adipocytes upon treatment with GH (20), GHR knockout mice exhibit increased numbers of sc adipocytes (82). Our investigations did not reveal significant modifications in the number of SAT LDs in *vizzini* mutants relative to wild-type controls; further analyses await the development of a transgenic line labeling zebrafish preadipocytes.

Mammalian GH is centrally involved in the use of stored lipid from adipose tissue, and GH stimulates lipolysis and lipid oxidation (26). Our in vivo imaging ap-

proach revealed a dramatic increase in size of SAT LDs in *vizzini* mutants compared with wild type, suggesting that lipolysis is deficient in *vizzini* SAT. Further, 21 days of starvation did not measurably decrease either the size or number of SAT LDs in *vizzini* mutants, suggesting that lipolysis and mobilization of adipose tissue are defective in *gh1* mutants and that, as in mammals, GH1 plays a critical role in lipid mobilization in teleosts.

The increased LD hypertrophy and greater total quantity of adipose tissue relative to size suggest *vizzini* may serve as a zebrafish model of human GH-mediated obesity. Several models of zebrafish obesity have previously been described (30, 83, 84). However, obesity in these models was defined only through measures of body mass and size, triglyceride levels, and adipose tissue histology and did not use in vivo imaging nor quantify effects on different adipose tissues. Therefore, to our knowledge, the analysis of adipose tissue growth in *vizzini* mutants in the current study is the most comprehensive cellular investigation of obesity in zebrafish.

Acknowledgments

We thank the members of the Parichy lab, specifically M. Bessee, O. Blackstone, P. Castro, C. Jones-Weinert, and S. Redmond.

Address correspondence and requests for reprints to: Dr. David M. Parichy, Department of Biology, University of Washington, Box 351800, Seattle, Washington 98195-1800. E-mail: dparichy@u.washington.edu. or Dr John F. Rawls, Department of cell Biology and physiology, University of North Carolina, Chapel Hill, North Carolina 27599. E-mail: john_rawls@med.unc.edu.

This work was supported by National Institutes of Health (NIH) Grants R01 HD040165 and R01 GM062182 and a grant from the University of Washington Royalty Research Foundation (D.M.P.), and by NIH Grant R56 DK091356 (to J.F.R.). S.K.M. was supported by the NIH National Research Service Award F32 (GM090362). J.E.N.M. was supported by the American Heart Association Postdoctoral Fellowship 11POST7360004.

Disclosure Summary: The authors have nothing to disclose.

References

1. Argente J, Caballo N, Barrios V, et al. Multiple endocrine abnormalities of the growth hormone and insulin-like growth factor axis in prepubertal children with exogenous obesity: effect of short- and long-term weight reduction. *J Clin Endocrinol Metab.* 1997;82:2076–2083.
2. Wabitsch M. Overweight and obesity in European children: definition and diagnostic procedures, risk factors and consequences for later health outcome. *Eur J Pediatr.* 2000;159:8–13.

3. Procter AM, Phillips JA, Cooper DN. The molecular genetics of growth hormone deficiency. *Hum Genet.* 1998;103:255–272.
4. Li CH, Simpson ME, Evans HM. Influence of growth and adrenocorticotrophic hormones on the body composition of hypophysectomized rats. *Endocrinology.* 1949;44:71–75.
5. Oberbauer A, Stern J, Johnson P, et al. Body composition of inactivated growth hormone (oMt1a-oGH) transgenic mice: generation of an obese phenotype. *Growth Dev Aging.* 1997;61:169.
6. Pomp D, Oberbauer AM, Murray JD. Development of obesity following inactivation of a growth hormone transgene in mice. *Transgenic Res.* 1996;5:13–23.
7. Waters M, Brooks A. Growth hormone receptor: structure function relationships. *Horm Res Paediatr.* 2011;76:12–16.
8. Han Y, Leaman DW, Watling D, et al. Participation of JAK and STAT proteins in growth hormone-induced signaling. *J Biol Chem.* 1996;271:5947–5952.
9. Wang X, Darus CJ, Xu BC, Kopchick JJ. Identification of growth hormone receptor (GHR) tyrosine residues required for GHR phosphorylation and JAK2 and STAT5 activation. *Mol Endocrinol.* 1996;10:1249–1260.
10. Savage MO, Burren CP, Rosenfeld RG. The continuum of growth hormone-IGF-I axis defects causing short stature: diagnostic and therapeutic challenges. *Clin Endocrinol (Oxf).* 2010;72:721–728.
11. Walenkamp MJE, Wit JM. Genetic disorders in the growth hormone-insulin-like growth factor-I axis. *Hormone Res.* 2006;66:221–230.
12. Forsyth IA, Wallis M. Growth hormone and prolactin—molecular and functional evolution. *J Mammary Gland Biol Neoplasia.* 2002;7:291–312.
13. Kawachi H, Suzuki K, Yamazaki T, et al. Identification of growth hormone in the sea lamprey, an extant representative of a group of the most ancient vertebrates. *Endocrinology.* 2002;143:4916–4921.
14. Reinecke M, Björnsson BT, Dickhoff WW, et al. Growth hormone and insulin-like growth factors in fish: where we are and where to go. *Gen Comp Endocrinol.* 2005;142:20–24.
15. Wallis M. The molecular evolution of vertebrate growth hormones: a pattern of near-stasis interrupted by sustained bursts of rapid change. *J Mol Evol.* 1996;43:93–100.
16. Zou S, Kamei H, Modi Z, Duan C. Zebrafish IGF genes: gene duplication, conservation and divergence, and novel roles in midline and notochord development. *PLoS One.* 2009;4:e7026.
17. Chen M, Huang X, Yuen DSH, Cheng CHK. A study on the functional interaction between the GH/PRL family of polypeptides with their receptors in zebrafish: evidence against GHR1 being the receptor for somatotactin. *Mol Cell Endocrinol.* 2011;337:114–121.
18. Sun K, Kusminski CM, Scherer PE. Adipose tissue remodeling and obesity. *J Clin Invest.* 2011;121:2094.
19. Kopelman PG. Obesity as a medical problem. *Nature.* 2000;404:635–643.
20. Bonnet F, Vanderschueren-Lodeweyckx M, Eeckels R, Malvaux P. Subcutaneous adipose tissue and lipids in blood in growth hormone deficiency before and after treatment with human growth hormone. *Pediatr Res.* 1974;8:800–805.
21. Bengtsson BÅ, Eden S, Lönn L, et al. Treatment of adults with growth hormone (GH) deficiency with recombinant human GH. *J Clin Endocrinol Metab.* 1993;76:309–317.
22. Salomon F, Cuneo RC, Hesp R, Sönksen PH. The effects of treatment with recombinant human growth hormone on body composition and metabolism in adults with growth hormone deficiency. *New Engl J Med.* 1989;321:1797–1803.
23. Morikawa M, Nixon T, Green H. Growth hormone and the adipose conversion of 3T3 cells. *Cell.* 1982;29:783–789.
24. Wabitsch M, Braun S, Hauner H, et al. Mitogenic and antiadipogenic properties of human growth hormone in differentiating human adipocyte precursor cells in primary culture1. *Pediatr Res.* 1996;40:450–456.
25. Wabitsch M, Heinze E, Hauner H, et al. Biological effects of human growth hormone in rat adipocyte precursor cells and newly differentiated adipocytes in primary culture. *Metabolism.* 1996;45:34–42.
26. Moller L, Dalman L, Norrelund H, et al. Impact of fasting on growth hormone signaling and action in muscle and fat. *J Clin Endocrinol Metab.* 2009;94:965–972.
27. Nam SY, Marcus C. Growth hormone and adipocyte function in obesity. *Horm Res Paediatr.* 2000;53:87–97.
28. Flynn EJ, Trent CM, Rawls JF. Ontogeny and nutritional control of adipogenesis in zebrafish (*Danio rerio*). *J Lipid Res.* 2009;50:1641–1652.
29. Elizondo MR, Budi EH, Parichy DM. Trpm7 regulation of in vivo cation homeostasis and kidney function involves stanniocalcin 1 and fgf23. *Endocrinology.* 2010;151:5700.
30. Song Y, Cone RD. Creation of a genetic model of obesity in a teleost. *FASEB J.* 2007;21:2042–2049.
31. Holtta-Vuori M, Salo V, Nyberg L, et al. Zebrafish: gaining popularity in lipid research. *Biochem J.* 2010;429:235–242.
32. Tingaud-Sequeira A, Ouadah N, Babin PJ. Zebrafish obesogenic test: a tool for screening molecules that target adiposity. *J Lipid Res.* 2011;52:1765–1772.
33. Imrie D, Sadler KC. White adipose tissue development in zebrafish is regulated by both developmental time and fish size. *Dev Dyn.* 2010;239:3013–3023.
34. Parichy DM, Elizondo MR, Mills MG, Gordon TN, Engeszer RE. Normal table of postembryonic zebrafish development: staging by externally visible anatomy of the living fish. *Dev Dyn.* 2009;238:2975–3015.
35. Minchin J, Rawls JF. In vivo analysis of white adipose tissue in zebrafish. *Methods Cell Biol.* 2011;105:63–86.
36. Solnica-Krezel L, Schier AF, Driever W. Efficient recovery of ENU-induced mutations from the zebrafish germline. *Genetics.* 1994;136:1401–1420.
37. Farmanfarmaian A, Sun LZ. Growth hormone effects on essential amino acid absorption, muscle amino acid profile, N-retention and nutritional requirements of striped bass hybrids. *Genet Anal: Biomol Eng.* 1999;15:107–113.
38. Shved N, Berishvili G, Mazel P, Baroiller JF, Eppler E. Growth hormone (GH) treatment acts on the endocrine and autocrine/paracrine GH/IGF-axis and on TNF- α expression in bony fish pituitary and immune organs. *Fish Shellfish Immunol.* 2011;31:944–952.
39. Raven P, Sakhrani D, Beckman B, et al. Growth and endocrine effects of recombinant bovine growth hormone treatment in non-transgenic and growth hormone transgenic coho salmon. *Gen Comp Endocrinol.* 2012;177:143–152.
40. Schneider CA, Rasband WS, Eliceiri KW. NIH image to ImageJ: 25 years of image analysis. *Nat Methods.* 2012;9:671–675.
41. Kimmel CB, Ballard WW, Kimmel SR, Ullmann B, Schilling TF. Stages of embryonic development of the zebrafish. *Dev Dyn.* 1995;203:253–310.
42. R Development Core Team. *R: A Language and Environment for Statistical Computing.* Vienna, Austria: R Foundation for Statistical Computing; 2012.
43. JMP. Version 8.0. Cary, North Carolina: SAS Institute, Inc; 2009.
44. Rozen S, Skaletsky HJ. Primer3 on the WWW for general users and for biologist programmers. Totowa, New Jersey: Humana Press; 2000.
45. Afonina I, Ankoudinova I, Mills A, Likhov S, Huynh P, Mahoney W. Primers with 5' flaps improve real-time PCR. *BioTechniques.* 2007;43:770–776.
46. Isaksson OGP, Edén S, Jansson JO, Lindahl A, Isgaard J, Nilsson A. Sites of action of growth hormone on somatic growth. *J Anim Sci.* 1986;63:48–56.
47. Laron Z. Insulin-like growth factor 1 (IGF-1): a growth hormone. *Mol Pathol.* 2001;54:311–316.

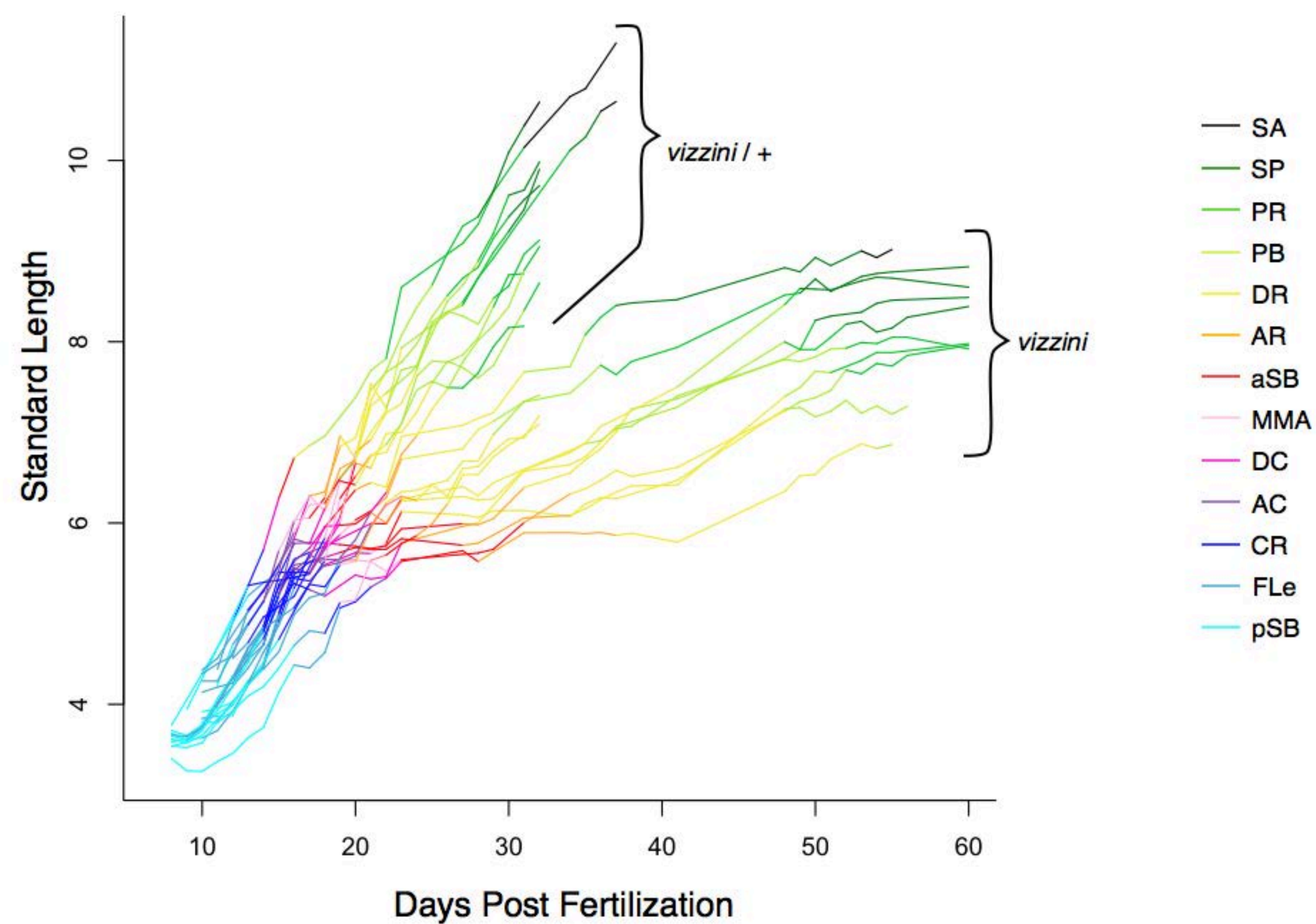
48. Wood AW, Duan C, Bern HA. Insulin-like growth factor signaling in fish. *Int Rev Cytol.* 2005;243:215–285.
49. Duan C. The insulin-like growth factor system and its biological actions in fish. *Am Zool.* 1997;37:491–503.
50. Shablott MJ, Cheng CM, Bolt D, Chen TT. Appearance of insulin-like growth factor mRNA in the liver and pyloric ceca of a teleost in response to exogenous growth hormone. *Proc Natl Acad Sci USA.* 1995;92:6943.
51. Davidson MB. Effect of growth hormone on carbohydrate and lipid metabolism. *Endocr Rev.* 1987;8:115–131.
52. Press M. Growth hormone and metabolism. *Diabetes Metab Rev.* 1988;4:391–414.
53. Berryman DE, List EO, Sackmann-Sala L, Lubbers E, Munn R, Kopchick JJ. Growth hormone and adipose tissue: beyond the adipocyte. *Growth Horm IGF Res.* 2011;21:113–123.
54. Palmer AJ, Chung MY, List EO, et al. Age-related changes in body composition of bovine growth hormone transgenic mice. *Endocrinology.* 2009;150:1353–1360.
55. Farese Jr RV, Walther TC. Lipid droplets finally get a little RESPECT. *Cell.* 2009;139:855–860.
56. Rodeheffer MS, Birsoy K, Friedman JM. Identification of white adipocyte progenitor cells in vivo. *Cell.* 2008;135:240–249.
57. Shen W, Wang ZM, Punyanita M, et al. Adipose tissue quantification by imaging methods: a proposed classification. *Obesity Res.* 2012;11:5–16.
58. Berryman DE, List EO, Coschigano KT, Behar K, Kim JK, Kopchick JJ. Comparing adiposity profiles in three mouse models with altered GH signaling. *Growth Horm IGF Res.* 2004;14:309–318.
59. Moreau D, Fleming I, Fletcher G, Brown J. Growth hormone transgenesis does not influence territorial dominance or growth and survival of first-feeding Atlantic salmon *Salmo salar* in food-limited stream microcosms. *J Fish Biol.* 2011;78:726–740.
60. Rahman MA, Maclean N. Growth performance of transgenic tilapia containing an exogenous piscine growth hormone gene. *Aquaculture.* 1999;173:333–346.
61. Devlin R, Johnsson J, Smailus D, Biagi C, Jönsson E, Björnsson BT. Increased ability to compete for food by growth hormone-transgenic coho salmon *Oncorhynchus kisutch* (Walbaum). *Aquacult Res.* 1999;30:479–482.
62. Mori T, Devlin RH. Transgene and host growth hormone gene expression in pituitary and nonpituitary tissues of normal and growth hormone transgenic salmon. *Mol Cell Endocrinol.* 1999;149:129–139.
63. Ofir R, Gootwine E. Ovine growth hormone gene duplication—structural and evolutionary implications. *Mamm Genome.* 1997;8:770–772.
64. Pogoda H-M, Hardt Svd, Herzog W, Krame C, Schwarz H, Hamerschmidt M. The proneural gene *ascl1a* is required for endocrine differentiation and cell survival in the zebrafish adenohypophysis. *Development.* 2011;133:1079–1089.
65. Zhu Y, Song D, Tran N-T, Nguyen N. The effects of the members of growth hormone family knockdown in zebrafish development. *Gen Comp Endocrinol.* 2007;150:395–404.
66. Gluckman PD, Pinal CS. Regulation of fetal growth by the somatotrophic axis. *J Nutr.* 2003;133:1741S–1746S.
67. Møller N, Jørgensen JOL. Effects of growth hormone on glucose, lipid, and protein metabolism in human subjects. *Endocr Rev.* 2009;30:152–177.
68. Jo J, Gavrilova O, Pack S, et al. Hypertrophy and/or hyperplasia: dynamics of adipose tissue growth. *PLoS Comp Biol.* 2009;5:e1000324.
69. Jo J, Guo J, Liu T, et al. Hypertrophy-driven adipocyte death overwhelms recruitment under prolonged weight gain. *Biophys J.* 2010;99:3535–3544.
70. MacKellar J, Cushman SW, Periwal V. Waves of adipose tissue growth in the genetically obese Zucker fatty rat. *PLoS One.* 2010;5:e8197.
71. Nishimura S, Manabe I, Nagasaki M, et al. In vivo imaging in mice reveals local cell dynamics and inflammation in obese adipose tissue. *J Clin Invest.* 2008;118:710.
72. Nishimura S, Manabe I, Nagasaki M, et al. Adipogenesis in obesity requires close interplay between differentiating adipocytes, stromal cells, and blood vessels. *Diabetes.* 2007;56:1517–1526.
73. Meyer CWE, Korthaus D, Jagla W, et al. A novel missense mutation in the mouse growth hormone gene causes semidominant dwarfism, hyperghrelinemia, and obesity. *Endocrinology.* 2004;145:2531–2541.
74. Zhou Y, Xu BC, Maheshwari HG, et al. A mammalian model for Laron syndrome produced by targeted disruption of the mouse growth hormone receptor/binding protein gene (the Laron mouse). *Proc Natl Acad Sci USA.* 1997;94:13215–13220.
75. Li S, Crenshaw EB, Rawson EJ, Simmons DM, Swanson LW, Rosenfeld MG. Dwarf locus mutants lacking three pituitary cell types result from mutations in the POU-domain gene *pit-1*. *Nature.* 1990;347:528–533.
76. Flurkey K, Papaconstantinou J, Miller RA, Harrison DE. Lifespan extension and delayed immune and collagen aging in mutant mice with defects in growth hormone production. *Proc Natl Acad Sci USA.* 2001;98:6736–6741.
77. Wabitsch M, Hauner H, Heinze E, Teller WM. The role of growth hormone/insulin-like growth factors in adipocyte differentiation. *Metabolism.* 1995;44:45–49.
78. Cotta OR, Santarpia L, Curtó L, et al. Primary growth hormone insensitivity (Laron syndrome) and acquired hypothyroidism: a case report. *JMCR.* 2011;5:301.
79. Guevara-Aguirre J, Balasubramanian P, Guevara-Aguirre M, et al. Growth hormone receptor deficiency is associated with a major reduction in pro-aging signaling, cancer, and diabetes in humans. *Sci Transl Med.* 2011;3:70ra13.
80. Li Y, Knapp JR, Kopchick JJ. Enlargement of interscapular brown adipose tissue in growth hormone antagonist transgenic and in growth hormone receptor gene-disrupted dwarf mice. *Exp Biol Med.* 2003;228:207–215.
81. Coschigano KT, Holland AN, Riders ME, List EO, Flyvbjerg A, Kopchick JJ. Deletion, but not antagonism, of the mouse growth hormone receptor results in severely decreased body weights, insulin, and insulin-like growth factor I levels and increased life span. *Endocrinology.* 2003;144:3799–3810.
82. Flint DJ, Binart N, Boumard S, Kopchick JJ, Kelly P. Developmental aspects of adipose tissue in GH receptor and prolactin receptor gene disrupted mice: site-specific effects upon proliferation, differentiation and hormone sensitivity. *J Endocrinol.* 2006;191:101–111.
83. Oka T, Nishimura Y, Zang L, et al. Diet-induced obesity in zebrafish shares common pathophysiological pathways with mammalian obesity. *BMC Physiol.* 2010;10:21.
84. Tainaka T, Shimada Y, Kuroyanagi J, et al. Transcriptome analysis of anti-fatty liver action by Campari tomato using a zebrafish diet-induced obesity model. *Nutr Metab.* 2011;8:88.

Supplemental Figure 1. Exogenous injection of rGH rescues somatic growth in vizzini mutants. A, schematic of the experimental design. Somatic growth, as measured by SL, was assessed after 9 days in the absence of rGH (-rGH) or presence of rGH (+rGH). rGH was administered intra-abdominally every 2 days at a concentration of 50 $\mu\text{g/g}$. B, on average vizzini mutants grew 0.48 mm more after supplementation with rGH ($P < 0.01$). N=4 vizzini, 5 wild-type.

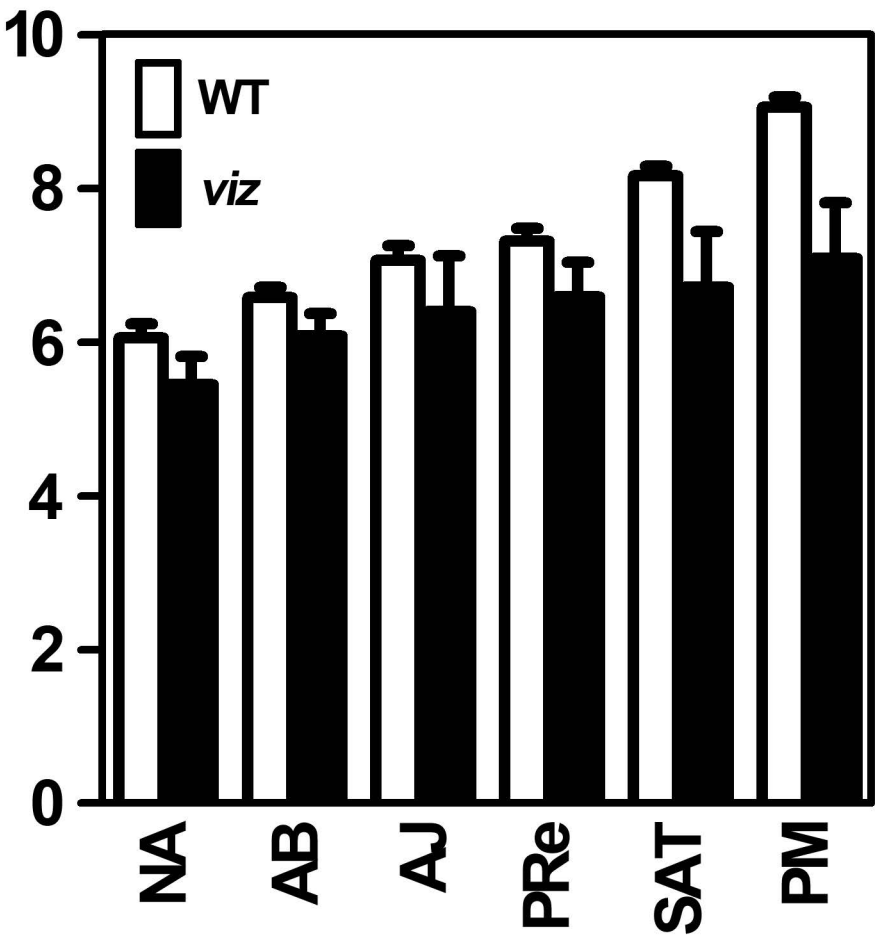
Supplemental Figure 2. vizzini mutants attain stages of post-embryonic development in their normal sequence, but do so at older ages than the wild-type. Stages of post-embryonic development are defined Fig. 2 (see 34); growth trajectory lines change colors as characters of each progressive stage were observed. N=643 observations; 11 wild-type, 13 vizzini mutants at series onset, with 5 wild-type and 5 vizzini mutants surviving to squamation (SP stage).

Supplemental Figure 3. vizzini mutants attain stages of adipose development in their normal sequence, but do so at sizes smaller than the wild-type. Shown are SL means ± 1 s.e.m. for ordered stages of adipose development. The sizes of vizzini mutants were significantly reduced in comparison to the wild-type overall (genotype, $F_{1,106}=12.6$, $P < 0.001$) and size differences between genotypes were accentuated for later stages (genotype x stage interaction, $F_{5,198}=5.2$, $P < 0.0001$). N=246 observations; 59 wild-type, 12 vizzini mutants. Stages are: NA, no adipose depot development; AB, appearance of abdominal adipose depot; AJ, joining of two initially distinct clusters of abdominal adipose tissue (compare abdominal tissue in Fig. 3E to that in Fig. 3H); PRe: appearance of perirenal adipose tissue; SAT: appearance of subcutaneous adipose tissue; PM: morphological change in pancreatic adipose shape with stereotyped anteriorward expansion (compare pancreatic tissue in Fig. 3H to that in Fig. 3K).

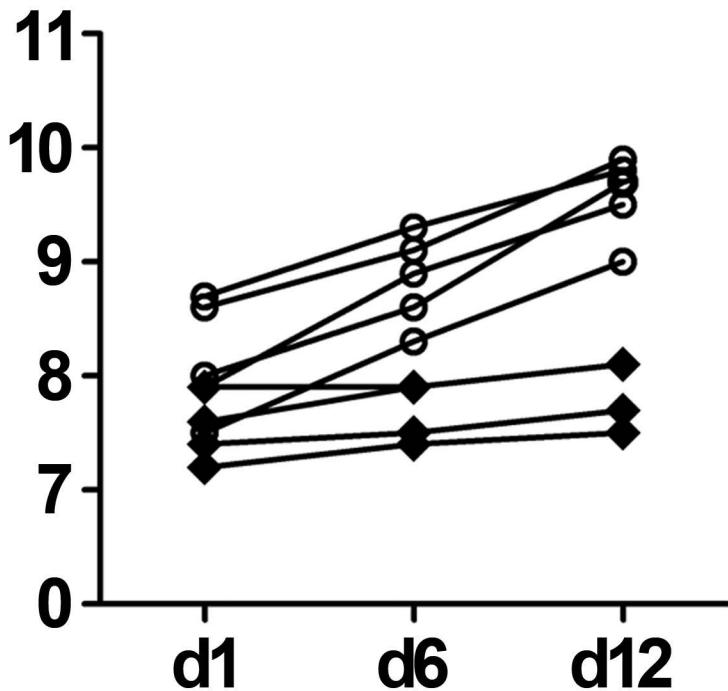
Supplemental Figure 4. Individual fish imaged longitudinally for adipose development grew at rates typical of their genotypes. d1, imaging day 1; d6, imaging day 6; d12; imaging day 12.



Standard Length (mm)



Standard Length (mm)



○ WT ($n=5$)

◆ *viz* ($n=4$)